Journal of Sound and Vibration 330 (2011) 416–430

Contents lists available at ScienceDirect

Journal of Sound and Vibration

journal homepage: www.elsevier.com/locate/jsvi

Sound generated by a vortex convected past an elastic sheet

A. Manela *

Faculty of Aerospace Engineering, Technion - Israel Institute of Technology, Haifa 32000, Israel

ARTICLE INFO

Article history:
Received 3 January 2010
Received in revised form
8 August 2010
Accepted 17 August 2010
Handling Editor: L. Huang
Available online 9 September 2010

ABSTRACT

We study the motion and sound generated when a line vortex is convected in a uniform low-Mach flow parallel to a thin elastic sheet. The linearized sheet motion is analyzed under conditions where the unforced sheet (in the absence of the line vortex) is stationary. The vortex passage above the sheet excites a resonance mode of motion, where the sheet oscillates at its least stable eigenmode. The sources of sound in the acoustic problem include the sheet velocity and fluid vorticity. It is shown that the release of trailing-edge vortices, resulting from the satisfaction of the Kutta condition, has two opposite effects on sound radiation: while trailing-edge vortices act to reduce the pressure fluctuations occurring owing to the direct interaction of the line vortex with the unperturbed sheet, they extend and amplify the acoustic signal produced by the motion of the sheet. The sheet motion radiates higher sound levels as the system approaches its critical conditions for instability, where the effect of resonance becomes more pronounced. It is argued that the present theory describes the essential mechanism by which sound is generated as a turbulent eddy is convected in a mean flow past a thin elastic airfoil.

1. Introduction

The dynamics of a thin elastic sheet subject to fluid loading is a classical problem in fluid–structure interactions and has been studied extensively over the years [1,2]. Apart from its fundamental significance, the problem has attracted growing interest owing to its relevance in modeling biological phenomena as well as addressing engineering applications. These include, among others, the dynamics of paper flutter and its importance in amending production processes in commercial printing [3]; the role of flapping motion in improving propulsive efficiency of swimming [4]; the relation between wavy body motions and turbulent drag reduction during locomotion [5]; the impact of flutter phenomenon on aircraft control [6]; and the potential use of flow-induced motion of flexible bodies as a source of "green" energy [7–9].

Motivated by the above and other studies, a major part of the works analyzing fluid–sheet interactions have considered the motion of a sheet subject to *uniform* axial flow. The dynamical problem in this case is governed by a balance between sheet inertia, elasticity and fluid loading. Linearized stability analyses have been carried out to determine the critical conditions for the onset of sheet motion [10–14]. Additional works have then considered the non-linear motion evolving at super-critical conditions [15–17].

The *forced* motion of a flexible thin body, resulting from unsteadiness of the incoming flow or other forms of external forcing, has been studied in a separate set of works. The problem to be solved in this case is qualitatively different from the one described above: instead of seeking for a non-trivial homogeneous solution, a private solution satisfying the particular

* Tel.: +972 48292237; fax: +972 48292030.
E-mail address: avshalom@aerodyne.technion.ac.il

0022-460X/$ - see front matter © 2010 Elsevier Ltd. All rights reserved.
doi:10.1016/j.jsv.2010.08.023

form of an inhomogeneous forcing term is required. Crighton and Oswell [18], Lucey [19] and Peake [20] considered the response of an elastic plate to a localized external force. Tang et al. [21] studied the effects of gravity and oscillating angle of attack on a plate motion. Golubev et al. [22] analyzed the response of a flexible airfoil to impinging gust, motivated by the severe effect this might have on light-weight micro-air-vehicles. Manela and Howe [23] revisited the classical flag problem and calculated the flag motion induced by the action of von-Kármán vortex street released from the flag cylindrical pole.

The counterpart *acoustic* problem, namely the calculation of sound produced by fluid–sheet interactions, has been studied as a simplified model problem for describing more complex phenomena. These include, among others, the sound produced during palatal snoring [11,24] and the effects of an acoustic field on the aerodynamic performances of micro-air-vehicle wings [25]. The sources of sound in this problem include the body motion and any vortical-flow components. Howe [26] focused on the case of a rigid (stationary) plate and studied the acoustic field produced by the interaction of an incident line vortex with the plate end-points. A later work [27] considered the case of a semi-infinite plate and focused on the noise produced by an elastic trailing-edge. Abrahams [28,29] studied the low-Mach acoustic scattering from a plate clamped at both edges and subject to heavy fluid loading. Dowling [30] extended Lighthill's theory to determine the noise induced by a turbulent boundary layer over a flexible surface. Crighton [31] investigated the relation between vibration and sound by applying a line force and geometrical inhomogeneities to the structure. Evers and Peake [32] studied the noise generated by the interaction of a gust with a rigid airfoil in transonic flow. Abrahams and Wickham [33] followed the work by Crighton and Oswell [18] and examined the sound produced by the response of an infinite plate to impulse forcing. Manela and Howe [14] calculated the sound produced by the flapping of a flag in uniform flow and studied the effect of boundary conditions on the onset of motion.

The fully *combined* effect of structure elasticity and incoming-flow unsteadiness on sound radiation has been examined in relatively few works. Howe [34] considered the problem qualitatively by assuming a simplified harmonic form for the body deflection and fluid loading. Shah and Howe [35] studied the sound produced when a line vortex translates over an infinite rib-stiffened elastic plate. More recently, Schäfer et al. [36] calculated numerically the sound produced by the interaction of a thin flexible plate, clamped at both ends, with turbulent flow excited by obstacles located upstream. The authors divided the contributions to the acoustic radiation into "structural vibration" and "stream noise" components and studied each of them separately using finite-difference schemes.

The objective of the present work is to analyze the mechanism of sound radiation resulting from the coupling between the motion of thin structures and stream-flow non-uniformities. We focus on the case of a finite sheet subject to small Mach-number flow, where the acoustic wavelength is considerably larger than the sheet length. We model the flow non-uniformity by an incident line vortex convected in the mean stream and interacting with the sheet. At first we analyze the linearized sheet motion forced by the vortex. The analysis is then applied to predict the far-field acoustic radiation, taking into account both structure dynamics and vortex-induced noise. By completing this calculation, we aim at providing a description of the essential mechanism by which sound is generated as a turbulent eddy is convected in a mean flow past a thin flexible airfoil. Such analysis may be useful in situations where both vortex flow and structure elasticity are important, as in the design of flapping-based active noise control systems for the reduction of blade–vortex interaction noise [37,38]; or in monitoring the acoustic signature of underwater vehicles in naval applications [39]. In addition, strong coupling between structure elasticity and flow vorticity is also common in insect flight, where low thickness-to-chord wing ratios enable significant active and passive flapping motions [40]. These motions result in the radiation of sound waves, responsible for a wide variety of noises known as "insect songs" [41,42]. In this context, the present theory supplies preliminary examination of the sound generated by the passive flow-induced motion of a thin wing.

The paper is organized as follows: in Section 2 the dynamical problem is formulated and analyzed. The acoustic radiation is calculated in Section 3. The results for both sheet dynamics and sound field are presented in Section 4. A summary of our conclusions is given in Section 5.

2. Dynamical problem

Consider a thin flexible sheet of thickness λ, length L, span l and mass per unit area $\rho_s\lambda$ clamped at one end and free at the other (Fig. 1). The sheet is subject to a parallel low-Mach high-Reynolds number uniform stream flow of speed U in the x_1-direction and to an incident line vortex of strength Γ parallel to its edge and in the negative x_3-direction (into the plane

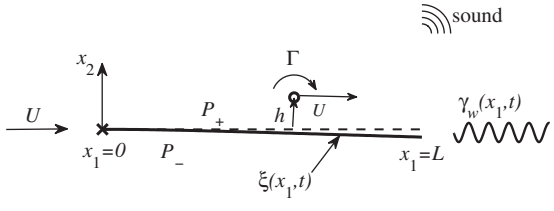

Fig. 1. Schematic setup of the problem. The sheet $\xi(x_1,t)$ is clamped at $x_1=0$ and free at $x_1=L$. The incident clockwise line vortex of strength Γ convects at the mean free stream U along $x_2=h$ and the inertial fluid loading on the sheet is $\Delta P=P_--P_+$.

of Fig. 1). It is assumed that the sheet length L is much smaller than its span l such that the motion may be regarded as two-dimensional. In addition, our analysis is based on linearized airfoil theory, where the vortex strength Γ is assumed sufficiently weak such that it is convected with the mean flow $\mathbf{U}=\hat{\mathbf{i}}U$ along a straight line $x_2=h$ parallel to the undisturbed sheet. For simplicity, we consider only the impact of the incident vortex on the body and neglect any back reaction of the body on the vortex. We define $t=0$ to be the time at which the vortex passes above the clamped ($x_1=0$) leading-edge of the body.

Under the above assumptions, small-amplitude unsteady deflections of the sheet in the x_2-direction of amplitude $\xi(x_1,t)\ll L$ are taken to satisfy the linearized equation

$$\rho_s\lambda\frac{\partial^2\xi}{\partial t^2}+EI\frac{\partial^4\xi}{\partial x_1^4}-\Delta P=0, \tag{1}$$

where EI is the sheet bending rigidity (E being Young's modulus and $I=\lambda^3/12(1-\sigma^2)$ the moment of inertia per unit span; σ is the Poisson ratio of the material) and ΔP denotes the pressure force exerted by the fluid across the sheet in the direction of increasing ξ. Following a previous study [23], the effect of boundary layer drag force is omitted, as its magnitude is small compared with all other forces in the present high Reynolds-number setup.

2.1. The fluid loading ΔP

In accordance with our linear theory assumption, the inertial pressure jump ΔP is determined as a superposition of the potential flow associated with the large-scale flow induced by the motion of the sheet, and the wake-induced flow, arising from vortices released from the trailing-edge of the filament. The corresponding velocity potential ϕ, satisfying the two-dimensional Laplace equation together with impermeability and proper far-field attenuation conditions, may be written as

$$\phi(\mathbf{x},t)=\int_S\frac{A(\mathbf{s},t)}{|\mathbf{x}-\mathbf{s}|}\,\mathrm{d}\mathbf{s}, \tag{2}$$

where $A(\mathbf{s},t)$ is a distribution of point sources representing the sheet and trailing-edge wake.

The modeling of fluid loading over thin bodies immersed in streaming flow has been the subject of many works. In what follows, we regard the sheet as a flexible wing and adopt the classical solution based on linearized thin-airfoil theory [43]. The solution applies conformal mapping technique and Söhngen's formula to express the pressure jump across the filament. According to the theory, the sheet surface and trailing-edge wake are represented by thin vortex sheets of vorticities

$$\boldsymbol{\omega}_\xi=\hat{\mathbf{k}}\delta(x_2)\gamma_\xi(x_1,t)\quad\text{and}\quad\boldsymbol{\omega}_w=\hat{\mathbf{k}}\delta(x_2)\gamma_w(x_1,t), \tag{3}$$

corresponding to the sheet ($0\le x_1\le L$) and wake ($L<x_1<\infty$) surfaces, respectively. Here δ denotes the Dirac delta function. The pressure jump across the sheet is given by

$$\Delta P(x_1,t)=\rho_0\left(U\gamma_\xi(x_1,t)+\frac{\partial}{\partial t}\int_0^{x_1}\gamma_\xi(s,t)\,\mathrm{d}s\right), \tag{4}$$

where ρ_0 is the fluid density. The actual value of $\gamma_\xi(x_1,t)$ is specified through the satisfaction of the impermeability condition on the sheet,

$$v_n(\xi(x_1,t))=\frac{\partial\xi}{\partial t}+U\frac{\partial\xi}{\partial x_1}=-\frac{1}{2\pi}\int_0^L\frac{\gamma_\xi(s,t)}{x_1-s}\,\mathrm{d}s-\frac{1}{2\pi}\int_L^\infty\frac{\gamma_w(s,t)}{x_1-s}\,\mathrm{d}s, \tag{5}$$

which couples the wake and sheet vorticity distributions. The amount of vorticity released at the trailing-edge wake is specified, in turn, through the Kutta condition, ensuring that the velocity at the sheet trailing-edge remains finite and that the pressure jump across the wake vanishes,

$$\Delta P_w(x_1,t)=\rho_0\left(U\gamma_w(x_1,t)+\frac{\partial}{\partial t}\int_0^L\gamma_\xi(s,t)\,\mathrm{d}s+\frac{\partial}{\partial t}\int_L^{x_1}\gamma_w(s,t)\,\mathrm{d}s\right)=0. \tag{6}$$

To obtain an expression for the pressure jump ΔP in terms of the sheet deflection $\xi(x_1,t)$, Eqs. (5) and (6) are solved to express $\gamma_\xi=\gamma_\xi(\xi(x_1,t);x_1,t)$. Substituting this result into (4) and then into (1) yield a single equation for the sheet deflection. The explicit expression for the Fourier decomposition of the pressure jump (4) as a function of the sheet deflection is given in (23).

2.2. The forced problem

The incident line vortex of strength Γ, convected at the mean flow velocity $\mathbf{U}=\hat{\mathbf{i}}U$ along $x_2=h$, is represented by the singular distribution of vorticity

$$\boldsymbol{\omega}_\Gamma=-\hat{\mathbf{k}}\Gamma\delta(x_2-h)\delta(x_1-Ut), \tag{7}$$

where $\hat{\mathbf{k}}$ is a unit vector in the positive x_3-direction (out of the plane of Fig. 1). The vortex (7) can be written in the form

$$\boldsymbol{\omega}_\Gamma = \int_{-\infty}^{\infty} \overline{\boldsymbol{\omega}}_\Gamma \exp[-\mathrm{i}\omega t]\,\mathrm{d}\omega, \tag{8}$$

where

$$\overline{\boldsymbol{\omega}}_\Gamma = -\frac{\Gamma}{2\pi U}\hat{\mathbf{k}}\delta(x_2-h)\exp[\mathrm{i}\omega x_1/U], \quad -\infty < x_1 < \infty. \tag{9}$$

The potential $\phi_{\overline{\omega}_\Gamma}$ induced by $\overline{\boldsymbol{\omega}}_\Gamma$ follows from the appropriate solution of Laplace's equation. This supplies

$$\phi_{\overline{\omega}_\Gamma} = -\frac{\Gamma}{4\pi\mathrm{i}\omega}\exp[\mathrm{i}\omega x_1/U + |\omega|(x_2-h)/U], \quad |x_2| < h. \tag{10}$$

This formula can be used to calculate the corresponding fluid displacement $\overline{\xi}_\Gamma$ induced at the mean position of the sheet by satisfying the kinematic condition

$$\frac{\mathrm{D}\overline{\xi}_\Gamma}{\mathrm{D}t} = -\mathrm{i}\omega\overline{\xi}_\Gamma + U\frac{\partial\overline{\xi}_\Gamma}{\partial x_1} = \frac{\partial\phi_{\overline{\omega}_\Gamma}}{\partial x_2}\bigg|_{x_2=0}, \tag{11}$$

or explicitly

$$-\mathrm{i}\omega\overline{\xi}_\Gamma + U\frac{\partial\overline{\xi}_\Gamma}{\partial x_1} = -\frac{\Gamma\,\mathrm{sign}(\omega)}{4\pi\mathrm{i}U}\exp\left[\mathrm{i}\omega x_1/U - |\omega|h/U\right]. \tag{12}$$

Integrate (12) and choose the particular solution

$$\overline{\xi}_\Gamma(x_1,\omega) = -\frac{\Gamma\,\mathrm{sign}(\omega)}{4\pi\mathrm{i}U^2}x_1\exp[\mathrm{i}\omega x_1/U - |\omega|h/U], \tag{13}$$

which vanishes at $x_1 = 0$. This choice of the particular solution, which is equivalent to setting the homogeneous response in (12) to zero, can be made without loss of generality as other choices of the constant of integration will not affect the final result for $\xi(x_1,t-x_1/U)$ (see (15) *et seq.*). The overall "vortex-induced" deflection $\xi_\Gamma(x_1,t-x_1/U)$ is given by integration of (13) over all frequencies $(-\infty,\infty)$

$$\xi_\Gamma(x_1,t-x_1/U) = \int_{-\infty}^{\infty}\overline{\xi}_\Gamma(x_1,\omega)\exp[-\mathrm{i}\omega t]\,\mathrm{d}\omega = -\frac{\Gamma x_1(t-x_1/U)}{2\pi U^2[(t-x_1/U)^2 + h^2/U^2]}. \tag{14}$$

Eq. (14) can now be used to formulate a "forced" equation of motion of the sheet in the presence of the incident line vortex. Let the overall sheet deflection ξ be partitioned into its "self" and "vortex-induced" parts

$$\xi(x_1,t-x_1/U) = \xi_o(x_1,t-x_1/U) + \xi_\Gamma(x_1,t-x_1/U) \tag{15}$$

and substitute this into (1). Note that in the linearized approximation the vortex convecting in the mean flow does not produce a pressure load on the sheet (see (10) at $x_2 = \pm 0$). The equation for ξ_o therefore assumes the inhomogeneous form

$$\rho_s\lambda\frac{\partial^2\xi_o}{\partial t^2} + EI\frac{\partial^4\xi_o}{\partial x_1^4} - \Delta P(\xi_o) = F_e(\xi_\Gamma), \tag{16}$$

where

$$F_e(\xi_\Gamma) = -\rho_s\lambda\frac{\partial^2\xi_\Gamma}{\partial t^2} - EI\frac{\partial^4\xi_\Gamma}{\partial x_1^4}. \tag{17}$$

Four boundary conditions are required to complete the formulation of the problem. We consider a clamped-free sheet setup, for which

$$(\xi)_{x_1=0} = \left(\frac{\partial\xi}{\partial x_1}\right)_{x_1=0} = \left(\frac{\partial^2\xi}{\partial x_1^2}\right)_{x_1=L} = \left(\frac{\partial^3\xi}{\partial x_1^3}\right)_{x_1=L} = 0, \tag{18}$$

requiring that the sheet displacement and slope vanish at the leading-edge, and the trailing-edge is moment- and force-free. The effect of boundary conditions different from (18) on the onset of motion and acoustic radiation of a flexible flag has been studied in Ref. [14]. It was found that when the clamped end is replaced by a supported end (i.e., the zero slope condition at $x_1 = 0$ is replaced by a zero moment condition), the stability properties of the system change considerably. However, no significant difference was found in the overall acoustic behavior between the clamped-free and supported-free cases. In the following we consider the clamped-free conditions (18) since they are most common in applications and can be studied in experiments relatively easily. Our analysis can be easily modified to study the impact of other boundary conditions.

The "forced" form of the boundary conditions is obtained by substituting (15) into (18), to yield

$$(\xi_o)_{x_1=0}=0,\quad \left(\frac{\partial\xi_o}{\partial x_1}\right)_{x_1=0}=-\left(\frac{\partial\xi_\Gamma}{\partial x_1}\right)_{x_1=0},\quad \left(\frac{\partial^2\xi_o}{\partial x_1^2}\right)_{x_1=L}=-\left(\frac{\partial^2\xi_\Gamma}{\partial x_1^2}\right)_{x_1=L},\quad \left(\frac{\partial^3\xi_o}{\partial x_1^3}\right)_{x_1=L}=-\left(\frac{\partial^3\xi_\Gamma}{\partial x_1^3}\right)_{x_1=L}. \tag{19}$$

Eqs. (16), (17) and (19) together with (14) complete the problem formulation for $\xi_o(x_1,t)$.

2.3. Analysis

To find the inhomogeneous solution of (16) we define the Fourier time transform $\overline{g}(x_1,\omega)$ of a function $g(x_1,t)$

$$\overline{g}(x_1,\omega)=\frac{1}{2\pi}\int_{-\infty}^{\infty}g(x_1,t)\exp[\mathrm{i}\omega t]\,\mathrm{d}t. \tag{20}$$

The transformed equation is

$$-\rho_s\lambda\omega^2\overline{\xi}_o+EI\overline{\xi}_o''''-\Delta\overline{P}(\overline{\xi}_o)=\overline{F}_e(\overline{\xi}_\Gamma), \tag{21}$$

where primes denote differentiation with x_1.

Explicit expression for the Fourier transform of the pressure jump, $\Delta\overline{P}(\overline{\xi}_o)$, is obtained by writing the Fourier decomposition of $\gamma_w(x_1,t)$ in (3) in the form

$$\overline{\gamma}_w(x_1,\omega)=\gamma_{w_0}(\omega)\exp[\mathrm{i}\omega x_1/U] \tag{22}$$

and following the steps outlined in Section 2.1. This yields [43]

$$\Delta\overline{P}(\overline{\xi}_o)=\frac{4\rho_0U}{\pi L}[1-C(L\omega/2U)]\sqrt{\frac{L-x_1}{x_1}}\int_0^L\sqrt{\frac{s}{L-s}}(-\mathrm{i}\omega\overline{\xi}_o+U\overline{\xi_o'})\,\mathrm{d}s+\frac{2\rho_0U}{\pi}\int_o^L\left[\sqrt{\frac{L-x_1}{x_1}}\sqrt{\frac{s}{L-s}}\frac{1}{x_1-s}+\frac{\mathrm{i}\omega}{U}\Lambda(x_1,s)\right](-\mathrm{i}\omega\overline{\xi}_o+U\overline{\xi_o'})\,\mathrm{d}s, \tag{23}$$

where

$$\Lambda(x_1,s)=\frac{1}{2}\log\left[\frac{Lx_1+Ls-2x_1s+2\sqrt{x_1(L-x_1)}\sqrt{s(L-s)}}{Lx_1+Ls-2x_1s-2\sqrt{x_1(L-x_1)}\sqrt{s(L-s)}}\right]. \tag{24}$$

The function $C(\omega)$, known as Theodorsen function [44], is given by

$$C(L\omega/2U)=\frac{H_1^{(2)}(L\omega/2U)}{H_1^{(2)}(L\omega/2U)+\mathrm{i}H_0^{(2)}(L\omega/2U)}, \tag{25}$$

where $H_n^{(m)}$ denotes the Hankel function of the mth kind and nth order.

The forcing term in (21) is

$$\overline{F}_e(\overline{\xi}_\Gamma)=\rho_s\lambda\omega^2\overline{\xi}_\Gamma-EI\overline{\xi_\Gamma''''}. \tag{26}$$

Substitute (13) into (26) to obtain

$$\overline{F}_e(\overline{\xi}_\Gamma)=-\frac{\Gamma\,\mathrm{sign}(\omega)}{4\pi\mathrm{i}U^2}\left[\rho_s\lambda\omega^2x_1-EI\left(-\frac{4\mathrm{i}\omega^3}{U^3}+\frac{\omega^4}{U^4}x_1\right)\right]\exp[\mathrm{i}\omega x_1/U-|\omega|h/U]. \tag{27}$$

The Fourier transform of the end conditions (19) is

$$\overline{\xi}_o(0)=-\overline{\xi}_\Gamma(0),\quad \overline{\xi_o'}(0)=-\overline{\xi_\Gamma'}(0),\quad \overline{\xi_o''}(L)=-\overline{\xi_\Gamma''}(L),\quad \overline{\xi_o'''}(L)=-\overline{\xi_\Gamma'''}(L). \tag{28}$$

The solution $\overline{\xi}_o(x_1,\omega)$ of the above problem is obtained numerically by the Chebyshev collocation method [45]. Once calculated, the "self" deflection of the sheet is given by the inverse Fourier transform

$$\xi_o(x_1,t-x_1/U)=\int_{-\infty}^{\infty}\overline{\xi}_o(x_1,\omega)\exp[-\mathrm{i}\omega t]\,\mathrm{d}\omega. \tag{29}$$

In practice, the infinite integral in (29) is confined to an integral over a finite interval. This is owing to the exponential decay of the integrand at large frequencies, resulting from the exponential dependence ($\sim\exp[-|\omega|h/U]$) of the forcing term (27).

The calculation of the total sheet displacement $\xi(x_1,t-x_1/U)$ is completed by taking the sum of (29) and (14) in (15).

3. Acoustic radiation

The acoustic pressure is given in the linearized approximation by the sum of four source-term contributions [46,47]

$$p(\mathbf{x},t)=p_{\xi_1}(\mathbf{x},t)+p_{\xi_2}(\mathbf{x},t)+p_{\Gamma_1}(\mathbf{x},t)+p_{\Gamma_2}(\mathbf{x},t). \tag{30}$$

In (30),

$$p_{\xi_1}(\mathbf{x},t)=\rho_0\frac{\partial}{\partial t}\int_{-\infty}^{\infty}\oint_{S_p}v_\perp(\mathbf{y},\tau)G_a(\mathbf{x},\mathbf{y},t-\tau)\,\mathrm{d}S(\mathbf{y})\,\mathrm{d}\tau \tag{31}$$

and

$$p_{\xi_2}(\mathbf{x},t)=-\rho_0\int_{-\infty}^{\infty}\int_{V_w}(\boldsymbol{\omega}_w\times\mathbf{U})\cdot\nabla G_a(\mathbf{x},\mathbf{y},t-\tau)\,\mathrm{d}^3\mathbf{y}\,\mathrm{d}\tau \tag{32}$$

are the pressure fluctuations resulting from the sheet motion and the outcome release of trailing-edge vorticity, respectively. Also appearing in (30) is

$$p_{\Gamma_1}(\mathbf{x},t)=-\rho_0\int_{-\infty}^{\infty}\int_{V_\Gamma}(\boldsymbol{\omega}_\Gamma\times\mathbf{U})\cdot\nabla G_a(\mathbf{x},\mathbf{y},t-\tau)\,\mathrm{d}^3\mathbf{y}\,\mathrm{d}\tau, \tag{33}$$

expressing the pressure perturbation produced by the interaction of the incident line vortex and the sheet, and its outcome trailing-edge vortex pressure contribution

$$p_{\Gamma_2}(\mathbf{x},t)=-\rho_0\int_{-\infty}^{\infty}\int_{V_\gamma}(\boldsymbol{\omega}_{\Gamma_v}\times\mathbf{U})\cdot\nabla G_a(\mathbf{x},\mathbf{y},t-\tau)\,\mathrm{d}^3\mathbf{y}\,\mathrm{d}\tau. \tag{34}$$

In (31)–(34), S_p is the sheet surface, $v_\perp(\mathbf{y},\tau)$ is the normal sheet velocity directed into the fluid,

$$v_\perp(\mathbf{y},t)=\pm\frac{\partial\xi}{\partial t}=\pm\frac{\partial\xi_o}{\partial t}\pm\frac{\partial\xi_\Gamma}{\partial t}\quad\text{on } y_2=\pm 0, \tag{35}$$

and $G_a(\mathbf{x},\mathbf{y},t-\tau)$ is the acoustic Green's function having a vanishing normal derivative on the undisturbed sheet. The volumes V_w and V_Γ denote the fluid regions occupied by the trailing-edge wake and the line vortex, respectively, and $\boldsymbol{\omega}_{\Gamma_v}$ is the vortex-induced trailing-edge vorticity (cf. (3))

$$\boldsymbol{\omega}_{\Gamma_v}=\hat{\mathbf{k}}\delta(y_2)\gamma_{\Gamma_v}(y_1,\tau). \tag{36}$$

When the Mach number based on the mean stream velocity is small enough that the sheet is acoustically compact, the compact approximation of Green's function [46,47]

$$G_a(\mathbf{x},\mathbf{y},t-\tau)=\frac{1}{4\pi|\mathbf{X}-\mathbf{Y}|}\delta\left(t-\tau-\frac{|\mathbf{X}-\mathbf{Y}|}{c_0}\right) \tag{37}$$

is applied to evaluate the far-field acoustic radiation. Here $\mathbf{X}(\mathbf{x})$ and $\mathbf{Y}(\mathbf{y})$ are the Kirchhoff vectors for the sheet and c_0 is the speed of sound. We approximate $\mathbf{Y}(\mathbf{y})$ by the Kirchhoff vector for a strip

$$\mathbf{Y}(\mathbf{y})=\left(y_1,\mathrm{Re}\left[-\mathrm{i}\sqrt{\left(y_1-\frac{L}{2}+\mathrm{i}y_2\right)^2-\frac{L^2}{4}}\right],y_3\right). \tag{38}$$

In what follows we focus on the far field ($|\mathbf{X}|\sim|\mathbf{x}|\to\infty$) radiation and approximate the above $G_a(\mathbf{x},\mathbf{y},t-\tau)$ by

$$G_a(\mathbf{x},\mathbf{y},t-\tau)\approx\frac{1}{4\pi|\mathbf{x}|}\delta\left(t-\tau-\frac{|\mathbf{x}|}{c_0}\right)+\frac{\mathbf{x}\cdot\mathbf{Y}}{4\pi c_0|\mathbf{x}|^2}\frac{\partial}{\partial t}\left[\delta\left(t-\tau-\frac{|\mathbf{x}|}{c_0}\right)\right],\quad|\mathbf{x}|\to\infty. \tag{39}$$

Note that while the analysis of the dynamical problem in Section 2 is strictly two-dimensional, the evaluation of the sound radiation is based on a three-dimensional formulation. This is made consistent by assuming a finite sheet span $l\gg L$ (see the beginning of Section 2) and neglecting any inhomogeneities in the spanwise direction caused by the sheet edges. Consequently, the description of the sheet motion is assumed to be independent of the spanwise location and any integration along the y_3-direction of the sheet in the acoustic problem is replaced by multiplication with its span l. The counterpart two-dimensional acoustic problem for a *rigid* plate, where the y_3-source coordinate extends to infinity, was studied by Howe in Refs. [26,46,47]. The results presented in Section 4.2.1 show that the present and Howe's calculation yield similar descriptions for the acoustic field generated in the rigid-plate case.

3.1. The sheet-motion sound

The "sheet-motion sound" corresponds in the following to the pressure fluctuations resulting directly from the sheet motion and its outcome trailing-edge wake,

$$p_\xi(\mathbf{x},t)=p_{\xi_1}(\mathbf{x},t)+p_{\xi_2}(\mathbf{x},t). \tag{40}$$

To calculate $p_{\xi_1}(\mathbf{x},t)$, substitute (39) into (31) to obtain

$$p_{\xi_1}(\mathbf{x},t)\approx\frac{\rho_0}{4\pi|\mathbf{x}|}\frac{\partial}{\partial t}\oint_{S_p}v_\perp(\mathbf{y},[t])\,\mathrm{d}S(\mathbf{y})+\frac{\rho_0 x_j}{4\pi c_0|\mathbf{x}|^2}\cdot\frac{\partial^2}{\partial t^2}\oint_{S_p}v_\perp(\mathbf{y},[t])Y_j(\mathbf{y})\,\mathrm{d}S(\mathbf{y}), \tag{41}$$

where $[t]=t-|\mathbf{x}|/c_0$ denotes the *acoustic retarded time*. The first integral, representing a monopole, vanishes because the volume of the sheet is constant. The leading order of the acoustic far field is therefore of a dipole type, determined by the second integral. Along the sheet $y_2=\pm 0$, $\mathrm{d}S=\mathrm{d}y_1\mathrm{d}y_3$, $0\le y_1\le L$ and $0\le y_3\le l$. Substitute (38) into (41) to obtain

$$p_{\xi_1}(\mathbf{x},t)\approx\frac{\rho_0 l x_2}{2\pi c_0|\mathbf{x}|^2}\frac{\partial^2}{\partial t^2}\int_0^L v_\perp(y_1,[t])\sqrt{y_1(L-y_1)}\,\mathrm{d}y_1. \tag{42}$$

Substituting (35) and the definition $x_2=|\mathbf{x}|\cos\theta$ (with $0\le\theta\le\pi$ indicating the observer direction) into (42) yields

$$p_{\xi_1}(|\mathbf{x}|,\theta,t)\approx\frac{\rho_0 l\cos\theta}{2\pi c_0|\mathbf{x}|}\frac{\partial^3}{\partial t^3}\int_0^L \xi(y_1,[t])\sqrt{y_1(L-y_1)}\,\mathrm{d}y_1. \tag{43}$$

To calculate $p_{\xi_2}(\mathbf{x},t)$, substitute (3) together with the inverse Fourier transform of (22) into (32) and expand for $|\mathbf{x}|\to\infty$. Following a procedure similar to the one carried out for $p_{\xi_1}(\mathbf{x},t)$, obtain

$$p_{\xi_2}(|\mathbf{x}|,\theta,t)\approx-\frac{\rho_0 Ul\cos\theta}{2\pi c_0|\mathbf{x}|}\frac{\partial}{\partial t}\int_{-\infty}^{\infty}\gamma_{w_0}(\omega)\mathrm{e}^{-\mathrm{i}\omega[t]}\int_L^\infty\left(\frac{\partial Y_2}{\partial y_2}\right)_{y_2=0}\exp\left[\frac{\mathrm{i}\omega y_1}{U}\right]\mathrm{d}y_1\,\mathrm{d}\omega, \tag{44}$$

where $\gamma_{w_0}(\omega)$ is determined from the satisfaction of the Kutta condition at the free end [43],

$$\gamma_{w_0}(\omega)=\frac{8\int_0^L\sqrt{\frac{s}{L-s}}[\mathrm{i}\omega\overline{\xi}(s,\omega)-U\overline{\xi}'(s,\omega)]\,\mathrm{d}s}{\pi L[H_1^{(2)}(L\omega/2U)+\mathrm{i}H_0^{(2)}(L\omega/2U)]}. \tag{45}$$

Making use of (38) we find

$$\left(\frac{\partial Y_2}{\partial y_2}\right)_{y_2=0}=\frac{y_1-L/2}{\sqrt{y_1(y_1-L)}}, \tag{46}$$

and the y_1-integration in (44) yields

$$\int_L^\infty\left(\frac{\partial Y_2}{\partial y_2}\right)_{y_2=0}\exp\left[\frac{\mathrm{i}\omega y_1}{U}\right]\mathrm{d}y_1=-\frac{\pi L}{2}\exp\left[\frac{\mathrm{i}L\omega}{2U}\right]H_1^{(1)}\left(\frac{L\omega}{2U}\right). \tag{47}$$

Substitute (47) and (45) into (44) to obtain

$$p_{\xi_2}(|\mathbf{x}|,\theta,t)\approx-\frac{\mathrm{i}\rho_0 Ul\cos\theta}{\pi c_0|\mathbf{x}|}\int_{-\infty}^{\infty}\frac{\omega H_1^{(1)}(L\omega/2U)}{H_1^{(2)}(L\omega/2U)+\mathrm{i}H_0^{(2)}(L\omega/2U)}\exp\left[-\mathrm{i}\omega\left([t]-\frac{L}{2U}\right)\right]\int_0^L\sqrt{\frac{s}{L-s}}[\mathrm{i}\omega\overline{\xi}(s,\omega)-U\overline{\xi}'(s,\omega)]\,\mathrm{d}s\,\mathrm{d}\omega. \tag{48}$$

The total sheet-motion acoustic pressure (40) is given by the sum of (43) and (48).

3.2. The incident-vortex sound

The "incident-vortex sound" corresponds in the following to the pressure perturbations caused by the vortex interaction with the unperturbed sheet and the subsequent release of trailing-edge vorticity,

$$p_\Gamma(\mathbf{x},t)=p_{\Gamma_1}(\mathbf{x},t)+p_{\Gamma_2}(\mathbf{x},t). \tag{49}$$

To evaluate $p_{\Gamma_1}(\mathbf{x},t)$ and $p_{\Gamma_2}(\mathbf{x},t)$, start by expressing $\boldsymbol{\omega}_\Gamma$ and $\boldsymbol{\omega}_{\Gamma_v}$ in (7) and (36) as linear arrays of harmonic line vortices,

$$\boldsymbol{\omega}_\Gamma=-\frac{\Gamma}{2\pi U}\hat{\mathbf{k}}\int_{-\infty}^{\infty}\delta(y_2-h)\exp\left[\mathrm{i}\omega\left(\frac{y_1}{U}-\tau\right)\right]\mathrm{d}\omega \tag{50}$$

and

$$\boldsymbol{\omega}_{\Gamma_v}=\hat{\mathbf{k}}\int_{-\infty}^{\infty}\delta(y_2)\gamma_{\Gamma_0}(\omega)\exp\left[\mathrm{i}\omega\left(\frac{y_1}{U}-\tau\right)\right]\mathrm{d}\omega. \tag{51}$$

The trailing-edge circulation per unit length $\gamma_{\Gamma_0}(\omega)$ is determined by the Kutta condition applied to the velocity field induced by the line vortex motion over the sheet [26]

$$\gamma_{\Gamma_0}(\omega)=\frac{\Gamma\,\mathrm{sign}(\omega)}{\pi U}\exp\left[-\frac{|\omega|h}{U}\right]\frac{J_0(\omega L/2U)+\mathrm{i}J_1(\omega L/2U)}{H_0^{(1)}(\omega L/2U)+\mathrm{i}H_1^{(1)}(\omega L/2U)}, \tag{52}$$

where J_n are Bessel functions of the first kind and nth order. Substitution of (50) and (51) into (33) and (34), respectively, together with the far-field approximation of Green's function (39), yield

$$p_{\Gamma_1}(\mathbf{x},t)\approx-\frac{\mathrm{i}\rho_0\Gamma l\cos\theta}{8\pi^2 c_0|\mathbf{x}|}\int_{-\infty}^{\infty}\omega\mathrm{e}^{-\mathrm{i}\omega[t]}\,\mathrm{d}\omega\int_{-\infty}^{\infty}\left(\frac{\partial Y_2}{\partial y_2}\right)_{y_2=h}\exp\left[\frac{\mathrm{i}\omega y_1}{U}\right]\mathrm{d}y_1 \tag{53}$$

and

$$p_{\Gamma_2}(\mathbf{x},t) \approx \frac{\mathrm{i}\rho_0 U l \cos\theta}{2\pi c_0 |\mathbf{x}|} \int_{-\infty}^{\infty} \omega \gamma_{\Gamma_0}(\omega) \mathrm{e}^{-\mathrm{i}\omega[t]} \mathrm{d}\omega \int_L^{\infty} \left(\frac{\partial Y_2}{\partial y_2}\right)_{y_2=0} \exp\left[\frac{\mathrm{i}\omega y_1}{U}\right] \mathrm{d}y_1. \tag{54}$$

The y_1-integrals in (53)–(54) can be calculated explicitly using (47) and contour integration. Substituting (52) into (54), the resulting $\omega-$integral expressions for p_{Γ_1} and p_{Γ_2} are

$$p_{\Gamma_1}(|\mathbf{x}|,\theta,t) \approx \frac{\mathrm{i}\rho_0 \Gamma l L \cos\theta}{8\pi c_0 |\mathbf{x}|} \int_{-\infty}^{\infty} \omega \,\mathrm{sign}(\omega) J_1\left(\frac{\omega L}{2U}\right) \exp\left[-\mathrm{i}\omega\left([t]-\frac{L}{2U}\right)-\frac{|\omega|h}{U}\right] \mathrm{d}\omega \tag{55}$$

and

$$p_{\Gamma_2}(|\mathbf{x}|,\theta,t) \approx -\frac{\mathrm{i}\rho_0 \Gamma l L \cos\theta}{8\pi c_0 |\mathbf{x}|} \int_{-\infty}^{\infty} \omega \;\mathrm{sign}(\omega) \frac{J_0(\omega L/2U)+\mathrm{i}J_1(\omega L/2U)}{H_0^{(1)}(\omega L/2U)+\mathrm{i}H_1^{(1)}(\omega L/2U)} H_1^{(1)}\left(\frac{\omega L}{2U}\right) \exp\left[-\mathrm{i}\omega\left([t]-\frac{L}{2U}\right)-\frac{|\omega|h}{U}\right] \mathrm{d}\omega. \tag{56}$$

The total incident-vortex acoustic pressure (49) is given by the sum of (55) and (56).

4. Results

4.1. Dynamical response

A non-dimensional representation of the problem is obtained by normalizing distances with the sheet length L and time with the convective time L/U. The problem is then governed by four non-dimensional parameters,

$$\mu = \frac{\rho_s \lambda}{\rho_0 L}, \quad \alpha = \frac{U}{U_b}, \quad R = \frac{h}{L} \quad \text{and} \quad \gamma = \frac{\Gamma}{UL}, \tag{57}$$

corresponding, respectively, to the normalized sheet mass density, wind speed (with $U_b = \sqrt{EI/\rho_s \lambda L^2} = \sqrt{E\lambda^2/12\rho_s L^2(1-\sigma^2)}$ being a characteristic bending wave speed), vortex–body distance and vortex strength. In consistence with our linear theory we focus on the case of a weak vortex ($\gamma \ll 1$) and fix $\gamma = 0.1$. Note that the sheet displacement is linear in γ and results for other values of $\gamma \ll 1$ can be obtained by simple manipulation of the data presented below. For later reference we focus on a parameter combination typical for insect wings, and take $\rho_s \approx 1100\,\mathrm{kg/m^3}$, $\lambda/L \approx 5\times10^{-3}$, $E \approx 100\,\mathrm{MPa}$ and $\sigma \approx 0.3$ [40,42]. Substituting these together with the value of air density $\rho_0 \approx 1.2\,\mathrm{kg/m^3}$ into μ and α in (57) yield $\mu \approx 4.5$ and $\alpha \approx U/0.45$ (U measured in SI units). This can be considered as a limit case of a very thin and flexible sheet; it should be noted, however, that similar qualitative results to those presented below are obtained for stiffer sheets with larger thickness ratios λ/L.

Our objective is to study the motion of the body forced by the incident line vortex. We therefore focus on conditions where the unforced flat sheet is stable to exclude any non-linear effects arising from coupling between the homogeneous and inhomogeneous sheet responses. The unforced sheet response has been studied in several works, both experimentally [3,11] and numerically [10–17]. For completeness, we calculated the critical conditions for instability according to our model. We skip the details of calculation here, as they are not the main focus of our work. Typically, the onset of sheet motion is characterized by a "neutral surface", marking the critical value of normalized wind speed $\alpha_c = \alpha_c(\mu, L\omega_c/U)$, above which sheet flapping starts. Fig. 2 presents the projections of the calculated neutral surface on the (μ,α) (Fig. 2a) and $(\mu, L\omega/U)$ (Fig. 2b) planes. According to our calculation, at $\mu = 4.5$ instability sets in for $\alpha_c \approx 6.5$ at a critical frequency of $L\omega_c/U \approx 2.97$. In what follows, we focus on subcritical conditions ($\alpha < \alpha_c$) and present results for $\alpha = 3, 5, 5.9$ and 6.3, marked by the circle, cross, triangle and square, respectively, in Fig. 2a. In reference to the above value of $U_b \approx 0.45\,\mathrm{m/s}$, these values of α correspond to a wind speed of $U < 2.9\,\mathrm{m/s}$, consistent with the low-Mach assumption set for the calculation of the sound radiation.

Before we turn to describe the forced sheet motion, some discussion of the expected behavior is in place. Schematically, we may write the self-induced plate motion ξ_o in the form

$$\xi_o(x_1, t-x_1/U) = \int_{-\infty}^{\infty} \frac{\overline{F}_{e_0}(x_1,\omega) \exp[-\mathrm{i}\omega(t-x_1/U)-|\omega|h/U]\,\mathrm{d}\omega}{D(\omega)}, \tag{58}$$

where $\overline{F}_{e_0}(x_1,\omega)$ is the function multiplying the exponent in (27), and $D(\omega)$ represents the dispersion relation characterizing the unforced sheet motion. While (58) may not be mathematically exact (owing to the x_1-dependence of the pressure jump operator in (21)), it gives some qualitative prediction of the expected results. Specifically, when the vortex is located at large distances from the sheet ($|x_1 - Ut| \to \infty$), the value of (58) is dominated by residue contributions from the poles of the integrand (i.e., the zeros of $D(\omega)$). Denoting the least stable pole by $\Omega = \Omega_r + \mathrm{i}\Omega_i$ and recalling that we

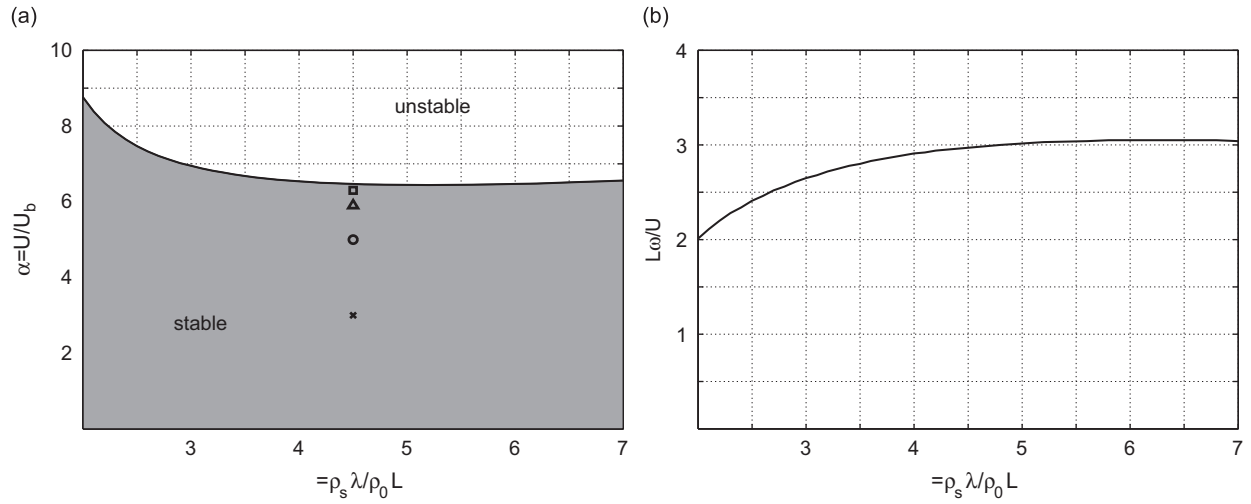

Fig. 2. The neutral surface $\alpha_c=\alpha_c(\mu,L\omega_c/U)$ for the unforced sheet problem: projections on the (a) (μ,α) and (b) $(\mu,L\omega/U)$ planes. The shaded zone in (a) marks the domain of stability and the line in (b) denotes the $\mu-$dependence of the critical flutter frequency at the onset of motion. The cross, circle, triangle and square correspond to the parameter combinations of $\mu=4.5$ and $\alpha=3,5,5.9,6.3$, respectively, considered in subsequent results for the forced motion and acoustic radiation.

focus on subcritical conditions ($\Omega_i<0$), we find that

$$\xi_o(x_1,t-x_1/U)\approx\begin{cases}\zeta_o\exp[\mathrm{i}\Omega_r(x_1/U-t)-\Omega_i(x_1/U-t)-|\Omega|h/U], & x_1-Ut\to-\infty,\\ 0, & x_1-Ut\to+\infty,\end{cases}\tag{59}$$

where ζ_o is determined by the residue of the integrand at the pole. The oscillatory motion at late times is therefore governed by the unforced eigenvalue frequency Ω_r and decay rate Ω_i, while it vanishes at early times. Moreover, the late-time resonance behavior predicted by (59) is expected to decay slower (and therefore to extend over a longer period of time) at subcritical conditions closer to the critical conditions of Fig. 2, owing to the decreasing value of $|\Omega_i|$.

Fig. 3 presents the time variation of the free-end displacement, $\xi(x_1/L=1,t)$, for $\mu=4.5$, R=1 and $\gamma=0.1$. The results are calculated at various subcritical values of α, corresponding to the points marked in Fig. 2a. The free-end has been chosen to represent the entire sheet motion. Similar results with reduced amplitudes were found at other points along the filament. At the lowest value of α presented ($\alpha=3$, Fig. 3a), the conditions are much below critical (see the cross in Fig. 2a). As a result, the value of $|\Omega_i|$ is too large to allow for any significant oscillations. At early times ($Ut/L\lesssim 0$), the displacement is small and negative in accordance with the clockwise velocity field induced by the vortex. Then, at $0\lesssim Ut/L\lesssim 5$, the close-field interaction between the vortex and the filament, not captured by (59), is reflected through a non-monotonic rapid change in the free-end displacement. At later times ($Ut/L\gtrsim 5$) the far-field approximation is recaptured and the sheet resumes its initial flat state.

Qualitatively different results are presented in Fig. 3b–d, where larger values of α are considered. Here, the late-time oscillatory motion of the sheet is clearly observed. The amplitude of oscillations increases with increasing α towards $\alpha_c\approx 6.5$, resulting from the decreasing value of $|\Omega_i|$. The frequency Ω_r of oscillations, reflecting the excitation of a resonance mode at the sheet least stable eigenmode, varies from $L\Omega_r/U\approx 3.89$ at $\alpha=5$, through $L\Omega_r/U\approx 3.25$ at $\alpha=5.9$, to $L\Omega_r/U\approx 3.07$ at $\alpha=6.3$. With further increasing α towards $\alpha_c\approx 6.5$, our results confirm that $L\Omega_r/U$ approaches the critical frequency of $L\omega_c/U\approx 2.97$. The close-field interaction of the vortex and the sheet becomes more complex at large α. In addition, the behavior at early times ($Ut/L\lesssim -5$) also includes oscillations at similar frequencies. It will be shown that these vibrations affect the resulting acoustic signature at early times (see Figs. 6 and 7).

To complement the above description, Fig. 4 shows the effect of non-dimensional vortex–body distance R on the free-end displacement. The results are presented for $\mu=4.5$, $\gamma=0.1$, $\alpha=5$ and three values of the non-dimensional vortex–body distance, $R=0.5,0.7$ and 1. With decreasing R, corresponding to a smaller vertical distance between the vortex and the body, the amplitude of motion increases while the frequency of oscillations remains nearly constant. This result is in accordance with the qualitative predictions of (59), where Ω_r is independent of R (since it does not appear in the unforced sheet problem) and the amplitude of motion is proportional to $\exp[-|\Omega|R]$ (the non-dimensional equivalent of $\exp[-|\Omega|h/U]$ in (59)).

In general, it is expected that the dynamical response of the filament should reflect the unforced (homogeneous) properties of the system. In the present subcritical investigation, the unforced sheet properties are manifested through a

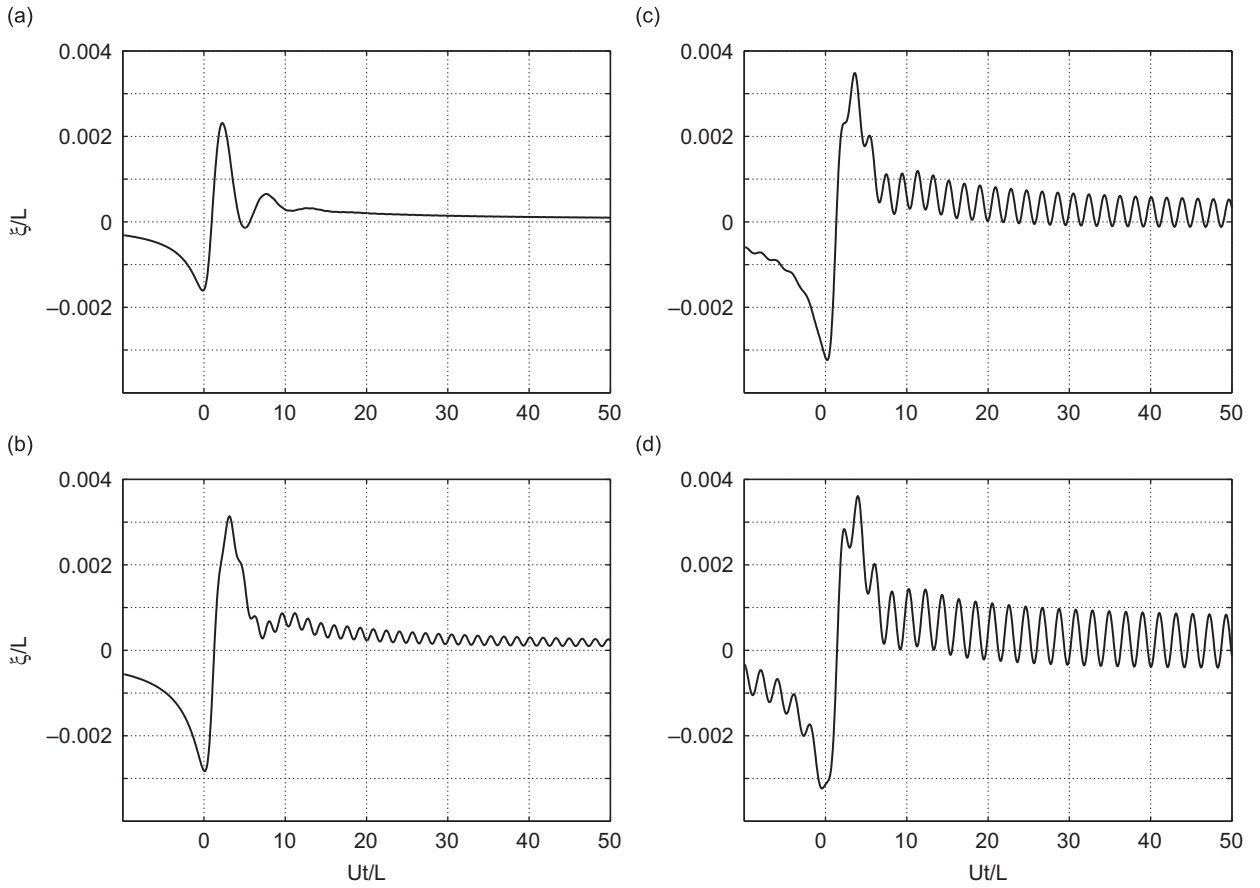

Fig. 3. The forced motion of the sheet trailing-edge ($x_1/L=1$) for $\mu=4.5$, $\gamma=0.1$, R=1 and (a) $\alpha=3$, (b) $\alpha=5$, (c) $\alpha=5.9$, (d) $\alpha=6.3$.

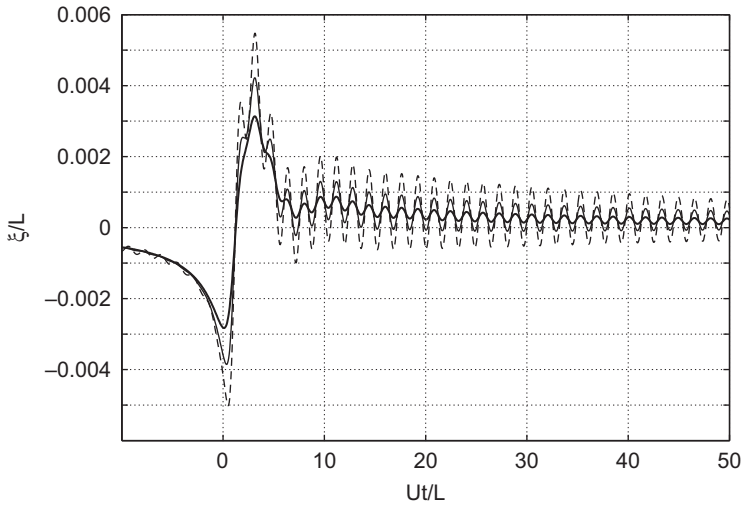

Fig. 4. The forced motion of the sheet free-end ($x_1/L=1$) for $\mu=4.5$, $\gamma=0.1$ and $\alpha=5$ at R=1 (bold line), R=0.7 (thin line) and R=0.5 (dashed line).

resonant mode excited by the infinite spectrum of the incident vortex. Owing to the subcritical conditions considered, this resonance behavior decays to zero at early and late times. This situation is expected to change qualitatively when considering the forced motion under super-critical ($\alpha>\alpha_c$) conditions, which may require a separate non-linear investigation.

4.2. Acoustic radiation

Following the non-dimensionalization introduced in Section 4.1, the normalized acoustic pressure (30) can be written as the sum of Eqs. (40) and (49),

$$\frac{p_\xi(|\mathbf{x}|,\theta,[t])}{\rho_0 U^2} = \frac{Ml\cos\theta}{2\pi|\mathbf{x}|}[F_{\xi_1}([\tilde{t}])+F_{\xi_2}([\tilde{t}])+F_{\Gamma_1}([\tilde{t}])+F_{\Gamma_2}([\tilde{t}])], \tag{60}$$

where $M = U/c_0 \ll 1$ are the mean stream Mach number and tildes denote non-dimensional quantities. Appearing in (60) is the scaled pressure components

$$F_{\xi_1}([\tilde{t}]) = \frac{\mathrm{d}^3}{\mathrm{d}\tilde{t}^3}\int_0^1 \tilde{\xi}(\tilde{y}_1,[\tilde{t}])\sqrt{\tilde{y}_1(1-\tilde{y}_1)}\,\mathrm{d}\tilde{y}_1, \tag{61}$$

$$F_{\xi_2}([\tilde{t}]) = -2\mathrm{i}\int_{-\infty}^{\infty}\tilde{\omega}\,\frac{\int_0^1\sqrt{\frac{s}{1-s}}[\mathrm{i}\tilde{\omega}\tilde{\tilde{\xi}}(s,\tilde{\omega})-\tilde{\tilde{\xi}}'(s,\tilde{\omega})]\,\mathrm{d}s}{H_1^{(2)}(\tilde{\omega}/2)+\mathrm{i}H_0^{(2)}(\tilde{\omega}/2)}H_1^{(1)}\left(\frac{\tilde{\omega}}{2}\right)\exp\left[-\mathrm{i}\tilde{\omega}\left([\tilde{t}]-\frac{1}{2}\right)\right]\mathrm{d}\tilde{\omega}, \tag{62}$$

$$F_{\Gamma_1}([\tilde{t}]) = \frac{\mathrm{i}\gamma}{4}\int_{-\infty}^{\infty}\tilde{\omega}\,\mathrm{sign}(\tilde{\omega})J_1\left(\frac{\tilde{\omega}}{2}\right)\exp\left[-\mathrm{i}\tilde{\omega}\left([\tilde{t}]-\frac{1}{2}\right)-|\tilde{\omega}|R\right]\mathrm{d}\tilde{\omega} \tag{63}$$

and

$$F_{\Gamma_2}([\tilde{t}]) = -\frac{\mathrm{i}\gamma}{4}\int_{-\infty}^{\infty}\tilde{\omega}\,\mathrm{sign}\,(\tilde{\omega})\frac{J_0(\tilde{\omega}/2)+\mathrm{i}J_1(\tilde{\omega}/2)}{H_0^{(1)}(\tilde{\omega}/2)+\mathrm{i}H_1^{(1)}(\tilde{\omega}/2)}H_1^{(1)}\left(\frac{\tilde{\omega}}{2}\right)\exp\left[-\mathrm{i}\tilde{\omega}\left([\tilde{t}]-\frac{1}{2}\right)-|\tilde{\omega}|R\right]\mathrm{d}\tilde{\omega} \tag{64}$$

originating from (43), (48), (55) and (56), respectively.

4.2.1. Incident-vortex sound

We start by examining the normalized pressure $F_\Gamma = F_{\Gamma_1}+F_{\Gamma_2}$ generated by the interaction of the vortex with the undisturbed sheet. This can be regarded as a limit case of a very "heavy" ($\mu \gg 1$) or "stiff" ($\alpha \ll 1$) sheet, where the vortex effects the sound radiation only through the release of trailing-edge vortices from the sheet free end. In this case both F_{ξ_1} and F_{ξ_2} vanish (as both ξ and its derivatives become negligibly small) and the only contributions to the sound arise from F_{Γ_1} and F_{Γ_2}.

Fig. 5 presents the retarded-time dependence of the scaled pressure components F_{Γ_1} and F_{Γ_2} (Fig. 5a, c) and their sum F_Γ (Fig. 5b, d) for $\gamma = 0.1$ and two vortex–plate distances, R=0.5 (Fig. 5a, b) and $R = 1$ (Fig. 5c, d). In all cases F_{Γ_1} and F_{Γ_2} vanish when the vortex is located upstream ($U[t]/L < -3$ in retarded-time units), consistent with the weak vortex–structure interaction at this stage. For R=0.5, as the incident vortex approaches the sheet leading-edge (at $U[t]/L \approx 0$), the pressure component F_{Γ_1}, associated with the direct vortex–body interaction, decreases sharply (solid line in Fig. 5a). Simultaneously, the associated trailing-edge wake component F_{Γ_2} increases, acting to reduce the pressure fluctuation generated by the direct interaction. This minimization of F_{Γ_1} is only partial: the vortex is located relatively far upstream ($x_1/L \approx 0$) from the sheet trailing-edge ($x_1/L = 1$) and the release of trailing-edge vortices does not suffice for complete sound cancellation. The effect of trailing-edge vortices becomes more pronounced when the vortex approaches $x_1/L = 1$: F_{Γ_1} and F_{Γ_2} nearly cancel out each other, leading to vanishingly small pressure fluctuations for $U[t]/L \geq 1$. This can be verified analytically by calculating the $R \ll 1$ approximations of F_{Γ_1} and F_{Γ_2} in (63) and (64), using the method of stationary phase [26]. Note that at the higher $R = 1$ case (Fig. 5c, d), significantly lower pressure levels occur and the acoustic signal extends over a wider time interval, owing to the less singular character of vortex–body interaction in this case.

Similar results to those in Fig. 5 were reported in Refs. [26,46,47], where a two-dimensional calculation of the acoustic field generated by the interaction between a line vortex and a rigid plate with infinite span was carried out (cf. Fig. 3.3.2 in Ref. [46]). In this respect, the present finite-span calculation is described mainly for validation of our theory and for easy reference to the following sheet-motion radiation analysis.

4.2.2. Sheet-motion sound

Fig. 6 shows the retarded-time dependence of the normalized acoustic pressure generated by the direct sheet motion F_{ξ_1}, its accompanying trailing-edge wake component F_{ξ_2} and their sum $F_\xi = F_{\xi_1}+F_{\xi_2}$ for $\mu = 4.5$, $\gamma = 0.1$ and $\alpha = 5$ (denoted by the circle in Fig. 2a). As in Fig. 5, two values of the non-dimensional vortex–sheet vertical distance R are presented: R=0.5 (Fig. 6a, b) and R=1 (Fig. 6c, d).

The total sheet-motion waveform F_ξ (Fig. 6b, d) is closely correlated to the forced motion presented in Section 4.1 and Fig. 4. At early times prior to the passage of the vortex above the sheet the acoustic signal vanishes. Small-amplitude oscillations are observed as the vortex approaches the sheet in the $R = 0.5$ case (Fig. 6b at $U[t]/L < 0$). These oscillations originate from the small (nearly invisible) counterpart forced-motion fluctuations (see the dashed line in Fig. 4 at $Ut/L < 0$). The acoustic signal undergoes rapid variations at "intermediate times", when the vortex passes above and close to the sheet ($0 \lesssim U[t]/L \lesssim 5$). These variations occur primarily owing to the trailing-edge wake component F_{ξ_2} (see below). At later

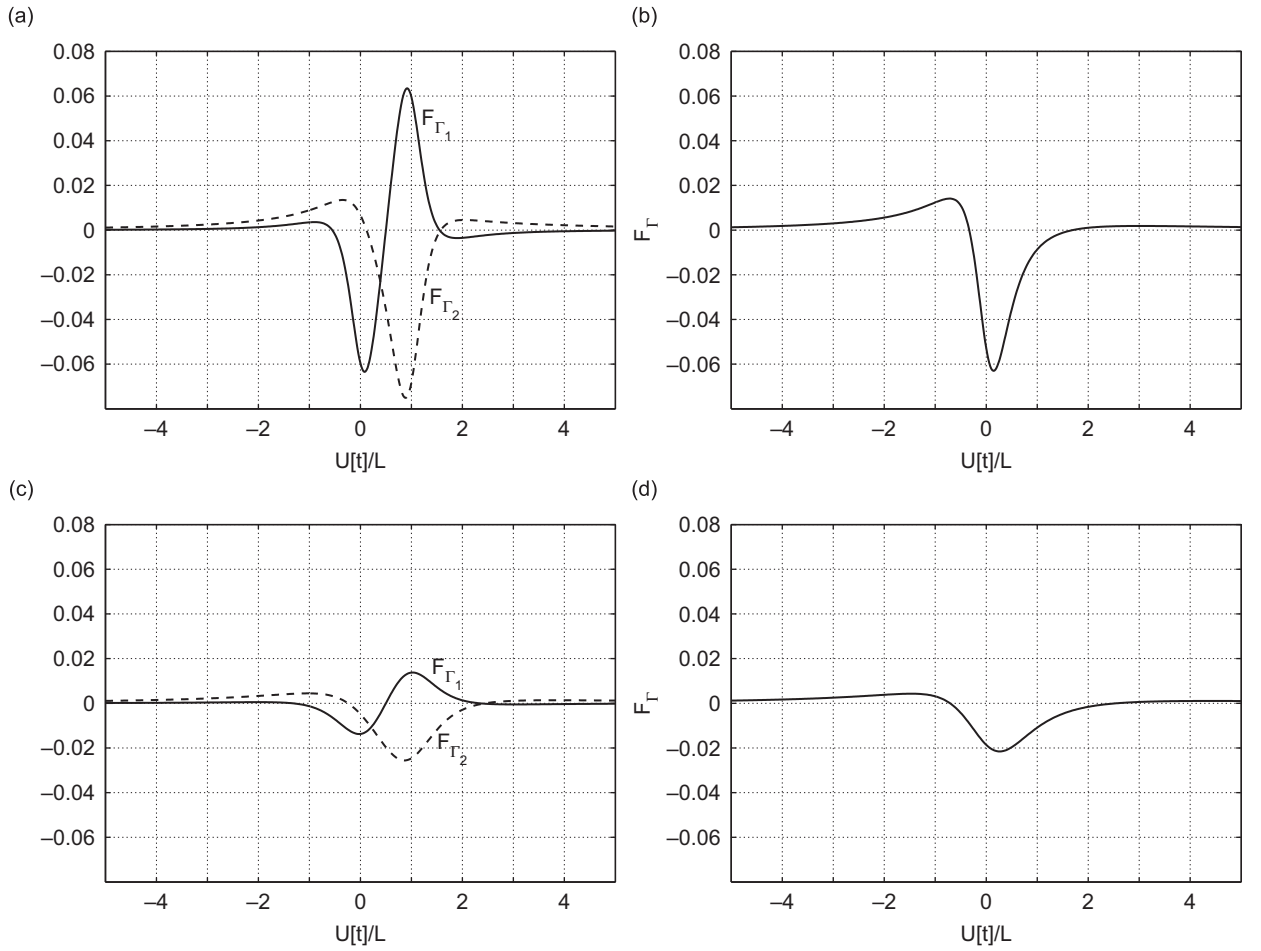

Fig. 5. The scaled acoustic pressure components (a,c) F_{Γ_1} (solid lines), F_{Γ_2} (dashed lines) and the total incident vortex pressure (b,d) $F_\Gamma = F_{\Gamma_1} + F_{\Gamma_2}$ for $\gamma = 0.1$ at (a,b) R=0.5 and (c,d) R=1.

times ($U[t]/L \gtrsim 5$), the acoustic pressure follows the resonance-motion behavior and is dominated by constant-frequency oscillations at the resonance frequency $L\Omega_r/U \approx 3.89$ found in Fig. 4. The amplitude of these oscillations decays with increasing time, in accordance with the qualitative prediction of Eq. (59).

The decomposition of F_ξ into F_{ξ_1} and F_{ξ_2} in Fig. 6a and 6c reveals an interesting feature: while F_{ξ_1} is responsible mainly for the late-time fluctuations, the trailing-edge wake component F_{ξ_2} is the dominant source of sound at intermediate times, when "close-field" sheet–vortex interactions take place. In contrast to the mechanism of trailing-edge noise cancellation found for a rigid plate (see Section 4.2.1), an opposite effect is revealed here: the trailing-edge component *adds* to the direct motion signal, resulting in increasing noise levels that extend over a longer period of time (see also Fig. 7). Our numerical calculations indicate that the increase in F_{ξ_2} at intermediate times stems from the relatively large values of trailing-edge vortex strength γ_{w_0}. Typically, when the vortex passes close to the sheet, the largest trailing-edge deflections occur. When these deflections are transmitted into sound, they are amplified through the square-root singularity of the s-integrand in (62). Physically, this is reflected through an increased release of trailing-edge vorticity (see (45)), which magnifies the relative effect of F_{ξ_2}.

Comparison between Figs. 5 and 6 presents two main differences between incident-vortex and sheet-motion sound: first, the sheet-motion signature is oscillatory, resulting from the excitation of the sheet resonance mode; second, the sound-motion noise extends over a time interval much longer than the incident-vortex signal. These differences become more evident with increasing α towards $\alpha_c \approx 6.5$. To demonstrate that, Fig. 7 shows the sheet-motion acoustic signature at $\mu = 4.5$, R=1 and $\alpha = 5.9$ (denoted by the triangle in Fig. 2). Owing to the larger value of α, the effect of resonance becomes more distinct, leading to sound levels larger than in the $\alpha = 5$ case (cf. Fig. 6c, d). In particular, the trailing-edge pressure contribution F_{ξ_2} becomes larger at both early and late times. This trend continues with increasing α towards $\alpha_c \approx 6.5$, where p_{ξ_2} becomes the main source of sound at all times. A similar finding was obtained in the study of the unforced flag sound [14], where the radiated acoustic field at critical conditions was dominated by the trailing-edge noise component. The mechanism here is similar to the one described above at intermediate times: at near-critical conditions the amplitude

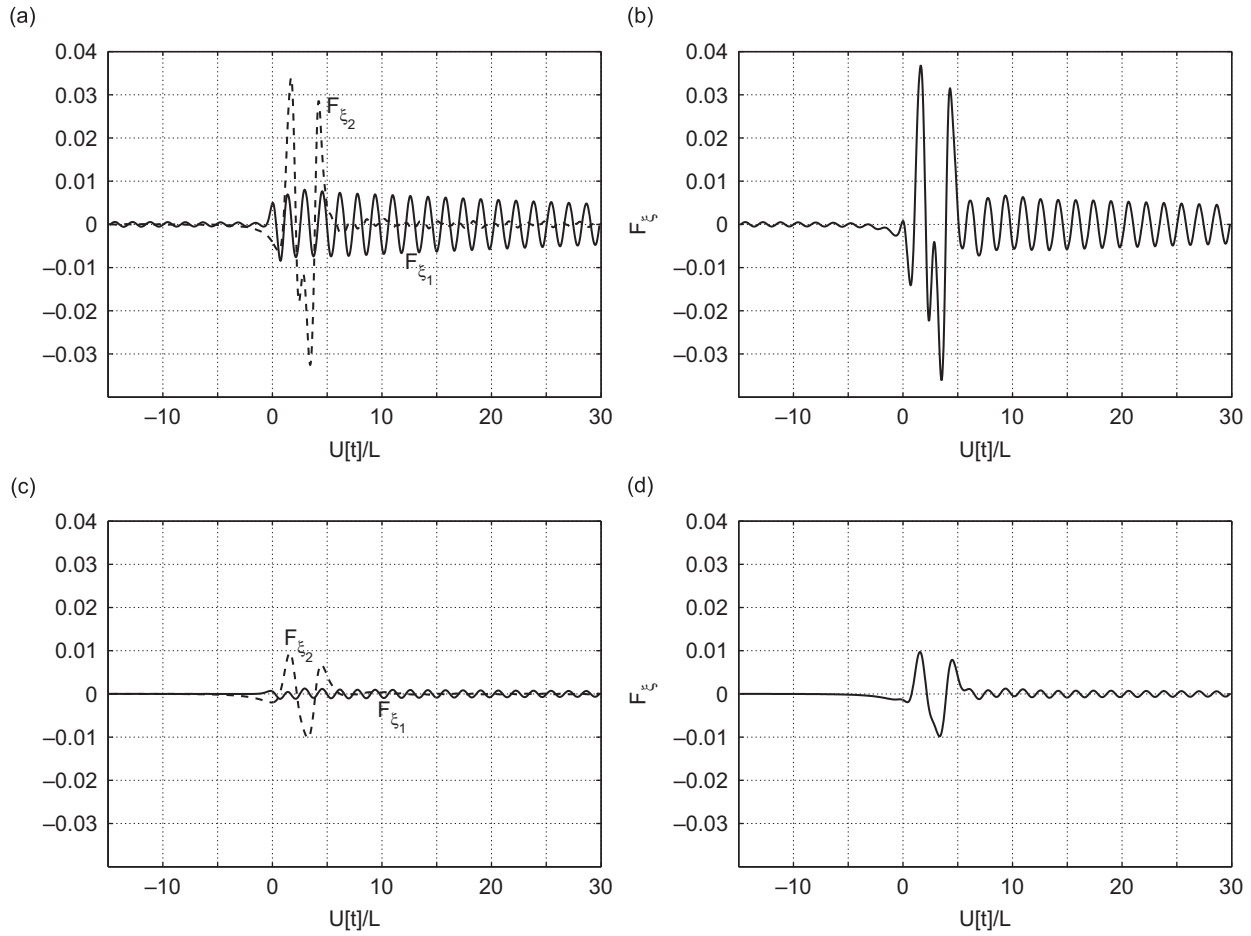

Fig. 6. The scaled acoustic pressure components (a,c) F_{ξ_1} (solid lines), F_{ξ_2} (dashed lines) and the total sheet-motion pressure (b,d) $F_\xi = F_{\xi_1} + F_{\xi_2}$ for $\mu = 4.5$, $\gamma = 0.1$ and $\alpha = 5$ at (a,b) R=0.5 and (c,d) R=1.

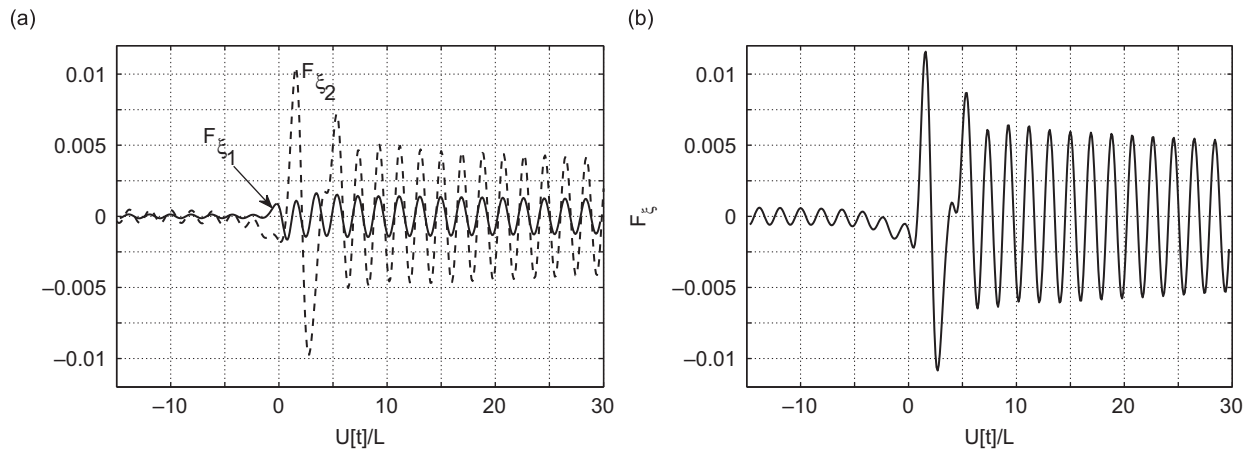

Fig. 7. The scaled acoustic pressure components: (a) F_{ξ_1} (solid line), F_{ξ_2} (dashed line) and the total sheet-motion pressure (b) $F_\xi = F_{\xi_1} + F_{\xi_2}$ for $\mu = 4.5$, $\gamma = 0.1$, $\alpha = 5.9$ and R=1.

of trailing-edge motion increases considerably, causing an increase in the release of trailing-edge vorticity. This increased vorticity levels, in turn, result in higher values of F_{ξ_2}.

To complement the examination of sheet-motion pressure signature, Fig. 8 shows the power spectrum magnitude of F_ξ for $\mu = 4.5$, $\gamma = 0.1$, $\alpha = 5.9$ and $R = 1$ (as in Fig. 7). The spectrum is normalized to have a maximum value of unity.

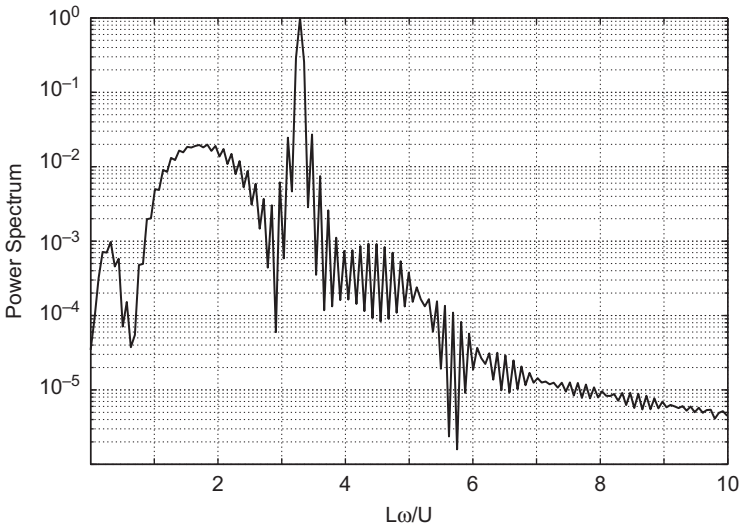

Fig. 8. Power spectrum of $F_\xi = F_{\xi_1} + F_{\xi_2}$ for $\mu = 4.5$, $\gamma = 0.1$, $\alpha = 5.9$ and $R = 1$.

As expected from the above results, the sheet-motion acoustic pressure is dominated by the resonance frequency $L\omega/U \approx 3.25$ found in Fig. 3c. Making use of the velocity-scale $U \approx 2.7\,\mathrm{m/s}$ (based on the values of $\alpha = U/U_b = 5.9$ and $U_b \approx 0.45\,\mathrm{m/s}$ estimated in the beginning of Section 4.1) and taking $L \approx 2\,\mathrm{cm}$ (typical chord size of insect wing), we find that the acoustic field in this case is dominated by sound of frequency $\omega/2\pi \approx 70\,\mathrm{Hz}$. Further investigation is required to study the acoustic field at higher supercritical values of α, where it is expected that the acoustic signature will become more complex and may include additional higher-frequency sound components.

5. Conclusion

We studied the motion and sound generated by the linearized interaction between a thin flexible sheet and an incident line vortex convected in a uniform stream. Analysis of the dynamical problem showed that the passage of the vortex above the sheet excites a resonance mode of motion, where the sheet oscillates at its least stable eigenmode. The magnitude of sheet motion decreases as the vortex is convected away from the sheet, in accordance with the decay rate of the respective eigenvalue.

The acoustic radiation in the compact-sheet case was formulated as a superposition of the ''incident-vortex noise'', resulting mainly from the interaction of the line vortex with the sheet end points, and the ''sheet-motion noise'', generated by the sheet motion. The satisfaction of the Kutta condition in each case revealed two opposite effects of trailing-edge vortices on sound production: while these vortices reduce the direct vortex–body interaction noise, they extend and amplify the sheet-motion sound radiation. The latter becomes increasingly dominant as the system approaches its critical conditions for instability, where the effect of resonance becomes more pronounced. Sheet-motion sound was found to be well correlated with the dynamical response of the structure. It is worthwhile to note that sound radiation of a resonance type, similar to the one found here, was also found by Howe in Ref. [34] (see Fig. 4 therein). In his work, the sound produced by the interaction of a line vortex with a spring-supported *rigid* plate was analyzed. Yet, the comparison between the two works can only be qualitative, owing to the different geometrical setups and boundary conditions considered.

Our analysis has focused on a case where the unforced sheet does not deflect; in other words, on conditions where the sheet motion is driven entirely by the incident vortex. The assumption made on the low strength of the vortex ($\gamma \ll 1$) enabled the use of superposition to describe the acoustic radiation as a sum over the various pressure contributions (30). A desirable extension of the present theory would therefore be an examination of the acoustic field at critical and supercritical conditions, where the homogeneous sheet response is not trivial, or in cases where the incident-vortex strength is large. Such analysis would require investigation of the non-linear problem, including a full coupling between the incident-vortex motion and sheet deflection. Additional study is also required for the extension of the present theory to the analysis of insect-flight sound. Apart from considering large-amplitude non-linear motion, such an extension may also incorporate the effect of active actuation of the structure (equivalent to active flapping of an insect wing), as well as incorporation of three-dimensional effects.

Acknowledgements

The author is indebted to Professor M.S. Howe for his valuable suggestions during discussions of this work and for commenting on the manuscript. The author is also thankful to Editor L. Huang, whose comments on the first version of this work have helped in improving the revised version of the paper.

References

[1] R.D. Blevins, *Flow-Induced Vibration*, Van Nostrand Reinhold, New York, 1990.
[2] M.P. Païdoussis, *Fluid–structure Interaction: Slender and Axial Flow*, Academic, London, 1998.
[3] Y. Watanabe, S. Suzuki, M. Sugihara, Y. Sueoka, An experimental study of paper flutter, *J. Fluids Struct.* 16 (2002) 529–542.
[4] J.C. Liao, D.N. Beal, G.V. Lauder, M.S. Triantafyllou, Fish exploiting vortices decrease muscle activity, *Science* 302 (2003) 1566–1569.
[5] L. Shen, X. Zhang, D.K.P. Yue, M.S. Triantafyllou, Turbulent flow over a flexible wall undergoing a streamwise traveling wave motion, *J. Fluid Mech.* 484 (2003) 197–221.
[6] R. De Breuker, M.M. Abdalla, Z. Gürdal, Flutter of partially rigid cantilevered two-dimensional plates in axial flow, *AIAA J.* 46 (2008) 936–946.
[7] G.W. Taylor, J.R. Burns, S.M. Kammann, W.B. Powers, T.R. Welsh, The energy harvesting eel: a small subsurface ocean/river power generator, *IEEE J. Ocean. Eng.* 26 (2001) 539–547.
[8] J.J. Allen, A.J. Smits, Energy harvesting eel, *J. Fluids Struct.* 15 (2001) 629–640.
[9] L. Tang, M.P. Païdoussis, J. Jiang, Cantilevered flexible plates in axial flow: energy transfer and the concept of flutter-mill, *J. Sound Vib.* 326 (2009) 263–276.
[10] A. Kornecki, E.H. Dowell, J. O'Brien, On the aeroelastic instability of two-dimensional panels in uniform incompressible flow, *J. Sound Vib.* 47 (1976) 163–178.
[11] L. Huang, Flutter of cantilevered plates in axial flow, *J. Fluids Struct.* 9 (1995) 127–147.
[12] M. Argentina, L. Mahadevan, Fluid-flow-induced flutter of a flag, *Proc. Natl. Acad. Sci.* 102 (2005) 1829–1834.
[13] C. Eloy, R. Lagrange, C. Souilliez, L. Schouveiler, Aeroelastic instability of cantilevered flexible plates in uniform flow, *J. Fluid Mech.* 611 (2008) 97–106.
[14] A. Manela, M.S. Howe, On the stability and sound of an unforced flag, *J. Sound Vib.* 321 (2009) 994–1006.
[15] B.H. Connell, D.K.P. Yue, Flapping dynamics of a flag in a uniform stream, *J. Fluid Mech.* 581 (2007) 33–67.
[16] L. Tang, M.P. Païdoussis, On the instability and the post-critical behaviour of two-dimensional cantilevered flexible plates, *J. Sound Vib.* 305 (2007) 97–115.
[17] S. Alben, M.J. Shelley, Flapping states of a flag in an inviscid fluid: bistability and the transition to chaos, *Phys. Rev. Lett.* 101 (2008) 119902.
[18] D.G. Crighton, J.E. Oswell, Fluid loading with mean flow. I. Response of an elastic plate to localized excitation, *Philos. Trans. R. Soc. London A* 335 (1991) 557–592.
[19] A.D. Lucey, The excitation of waves on a flexible panel in a uniform flow, *Philos. Trans. R. Soc. London A* 356 (1998) 2999–3039.
[20] N. Peake, On the unsteady motion of a long fluid-loaded elastic plate with mean flow, *J. Fluid Mech.* 507 (2004) 335–366.
[21] L. Tang, M.P. Païdoussis, J. Jiang, The dynamics of variants of two-dimensional cantilevered flexible plates in axial flow, *J. Sound Vib.* 323 (2009) 214–231.
[22] V.V. Golubev, B.D. Dreyer, T.M. Hollenshade, M.R. Visbal, High-accuracy viscous analysis of unsteady flexible airfoil response to impinging gust, AIAA paper No. 2009-3271, 2009.
[23] A. Manela, M.S. Howe, The forced motion of a flag, *J. Fluid Mech.* 635 (2009) 439–454.
[24] L. Huang, Mechanical modeling of palatal snoring, *J. Acoust. Soc. Am.* 97 (1995) 3642–3648.
[25] T.M. Grundy, G.P. Keefe, M.V. Lowson, Effects of acoustic disturbances on low *Re* aerofoil flows, *Prog. Astron. Aerosp.* 195 (2001) 91–113.
[26] M.S. Howe, The influence of vortex shedding on the generation of sound by convected turbulence, *J. Fluid Mech.* 76 (1976) 711–740.
[27] M.S. Howe, Structural and acoustic noise produced by turbulent noise over an elastic trailing edge, *Proc. R. Soc. London A* 442 (1993) 533–554.
[28] I.D. Abrahams, Scattering of sound by a heavily loaded finite elastic plate, *Proc. R. Soc. London* 378 (1981) 89–117.
[29] I.D. Abrahams, Scattering of sound by an elastic plate with flow, *J. Sound Vib.* 89 (1983) 213–231.
[30] A.P. Dowling, Flow-acoustic interaction near a flexible wall, *J. Fluid Mech.* 128 (1983) 181–198.
[31] D.G. Crighton, The 1988 Rayleigh medal lecture: fluid-loading—the interaction between sound and vibration, *J. Sound Vib.* 133 (1989) 1–27.
[32] I. Evers, N. Peake, Noise generation by high-frequency gusts interacting with an airfoil in transonic flow, *J. Fluid Mech.* 411 (2000) 91–130.
[33] I.D. Abrahams, G.R. Wickham, On transient oscillations of plates in moving fluids, *Wave Motion* 33 (2001) 7–24.
[34] M.S. Howe, Elastic blade-vortex interaction noise, *J. Sound Vib.* 177 (1994) 325–336.
[35] P.L. Shah, M.S. Howe, Sound generated by a vortex interacting with a rib-stiffened elastic plate, *J. Sound Vib.* 197 (1996) 103–115.
[36] F. Schäfer, T. Uffinger, S. Becker, J. Grabinger, M. Kaltenbacher, Fluid–structure interaction and computational aeroacoustics of the flow past a thin flexible structure, *Proceedings of the Acoustics 2008 Conference*, Paris, 2008, pp. 3755–3760 (see also J. Acoust. Soc. Am. 123 (2008) 3570.).
[37] M. Marcolini, E. Booth, H. Tadghighi, H. Hassan, C. Smith, L. Becker, Control of BVI noise using an active trailing edge flap, *Vertical Lift Aircraft Design Conference*, San Francisco, CA, 1995.
[38] K. Nguyen, M. Betzina, C. Kitaplioglu, Full-scale demonstration of higher harmonic control for noise and vibration reduction on the XV-15 rotor, *American Helicopter Society 56th Annual Forum*, Virginia Beach, VA, 2000.
[39] P.R. Bandyopadhyay, Maneuvering hydrodynamics of fish and small underwater vehicles, *Integ. Comput. Biol.* 42 (2002) 102–117.
[40] T. Maxworthy, The fluid dynamics of insect flight, *Ann. Rev. Fluid Mech.* 13 (1981) 329–350.
[41] H.C. Bennet-Clark, Acoustics of insect song, *Nature* 234 (1971) 255–259.
[42] S. Drosopoulos, M.F. Claridge (Eds.), *Insect Sounds and Communication: Physiology, Behaviour, Ecology and Evolution*, Taylor and Francis, Boca Raton, Florida, 2006.
[43] R.L. Bisplinghoff, H. Ashley, R.L. Halfman, *Aeroelasticity*, Addison-Wesley, Toronto, 1955.
[44] T. Theodorsen, General theory of aerodynamic instability and the mechanism of flutter, NACA Report no. 496, 1935.
[45] R. Peyret, *Spectral Methods for Incompressible Viscous Flow*, Springer, New-York, 2002.
[46] M.S. Howe, *Acoustics of Fluid–structure Interactions*, Cambridge University Press, Cambridge, 1998.
[47] M.S. Howe, *Theory of Vortex Sound*, Cambridge University Press, Cambridge, 2003.